

843. Efficient modeling and simulations of Lamb wave propagation in thin plates by using a new spectral plate element

Chunling Xu¹, Xinwei Wang²

State Key Laboratory of Mechanics and Control of Mechanical Structures

Nanjing University of Aeronautics and Astronautics, No. 29 Yudao Street, Nanjing 210016, China

E-mail: ¹yifxcl@126.com, ²wangx@nuaa.edu.cn

(Received 20 April 2012; accepted 4 September 2012)

Abstract. A new spectral plate element is presented for modeling selectively or simultaneously the symmetric and/or anti-symmetric modes of Lamb waves propagating in thin plate structures. The Legendre polynomials and the extended form of the displacement field are used in the formulation. The diagonal mass matrix is obtained by using a simple method with less computational effort. Detailed derivations are provided. Comparisons with existing results are performed to validate the formulations as well as the written programs. Numerical calculations have been carried out for thin aluminum plates with and without damages by using the proposed spectral plate element. Comparisons reveal that the proposed spectral plate element is more effective than the spectral plate element based on Chebyshev polynomials and the 3-D spectral finite elements with the same order of Legendre polynomials as the shape functions.

Keywords: spectral plate element, wave propagation, Lamb wave, damage identification.

1. Introduction

It is well known that detection of small damage in structures is an important but a challenging task in engineering practice. Thus, it is a hot research topic in the area of the structural health monitoring (SHM). To develop effective Lamb wave based SHM systems it is important to understand thoroughly the behavior of the Lamb wave propagation in structures with and without damages either experimentally or numerically. It is known, however, that the conventional finite element method (FEM) is computationally inefficient in analyzing elastic wave propagations [1]. Therefore, research efforts have been focused on developing efficient numerical algorithms for solutions of elastic Lamb propagations for the past few decades and are still underway. Various numerical algorithms reported in the literature, to list only a few, include the boundary element method (BEM) [2], the mass-spring lattice models (MSLM) [3], the local interaction simulation approach (LISA) [4], the discrete singular convolution (DSC) algorithm [5], and the spectral finite element method (SFEM) [6-10].

For the spectral finite element (SFE) methods, there are two different kinds of methods available, namely, the fast Fourier transform based SFE and the orthogonal-polynomial-based SFE. Research works show that the SFE method based on the orthogonal polynomials is much more suitable for analyzing wave propagation in structures with complex geometry than the FFT-bases method. The orthogonal-polynomial-based SFE method is similar to the classical finite element method in the assemblage of structural mass and stiffness matrices, as well as the solution procedures. If the shape functions are Legendre polynomial, the mass matrix is approximately in a diagonal form, a remarkable advantage over the conventional finite element method [1]. Therefore, the orthogonal-polynomial-based SFE method has been widely used to simulate wave propagation in structures for damage detection [11-15]. Kudela et al. [11] studied the wave propagation in 1-D structures by using the Legendre-polynomial-based SFE method. Zak et al. [12] investigated wave propagation in plates with a crack by using 2-D spectral finite element and identified the crack through the transmitted and reflected waves. Peng et al. [13] investigated the wave propagation in plates by using a 3-D spectral element. Based on

Mindlin's theory, Kudela et al. [14] studied the wave propagation in composite plates. Recently, Zak [15] proposed an extended form of the displacement field and presented a 2-D new spectral plate element. The attractive feature of the 2-D plate element is that it can model selectively or simultaneously the symmetric and/or anti-symmetric modes of Lamb waves propagating in plate structures. In other words, the 2-D plate element has the capability of a 3-D spectral element [13] in modeling the wave propagations in plates. Compared to the 3-D spectral element, the 2-D plate element is simpler and more computationally efficient.

It is noted that, however, the mass matrix of the novel plate element in [15] is not in a diagonal form. Therefore, additional effort has to be made in order to allow crucial reduction of the complexity and the cost of the time integration by using the central finite difference method. To remove this deficiency and raise the computational efficiency further, a modified spectral plate element is proposed herein. Instead of the Chebyshev polynomials used in [15], the Legendre polynomials are used as the shape functions and a simple method is used to formulate the diagonal mass matrix. These modifications will raise the critical time step (the largest time step for stable time integration) more than 80 % over that of the original plate element.

Formulations and solution procedures are worked out in detail. To validate the formulations, the written programs, as well as the computational efficiency, several examples are analyzed by using the proposed plate element. Numerical results are compared with existing (recalculated) data by using the 2-D spectral plate element in [15] and 3-D spectral element in [13]. Based on the results reported herein, some conclusions are drawn.

2. Formulations of the new spectral plate element

2.1 Definition of element nodes

It is known that in the formulation of a time-based spectral finite element, the nodal coordinates of an element are a key factor that strongly influences the element performance [15]. Different from the conventional finite element, nodes are distributed non-uniformly in the element. For the efficiency considerations, the nodal coordinates of the element in the element local coordinate system $\xi\eta$ are defined as the roots of the following polynomials [11]:

$$(1 - \xi^2)P'_N(\xi) = 0; (1 - \eta^2)P'_N(\eta) = 0 \quad (1)$$

where $\xi, \eta \in [-1, 1]$, $P'_N(\xi)$ and $P'_N(\eta)$ denote the first derivative of Legendre polynomials of degree N .

If the fifth order polynomials ($N = 5$) are chosen, the nodal coordinates of the element can be specified by:

$$\left. \begin{array}{l} \xi_1 \text{ (or } \eta_1) = -1 \\ \xi_2 \text{ (or } \eta_2) = -0.7650553239 \\ \xi_3 \text{ (or } \eta_3) = -0.2852315165 \\ \xi_4 \text{ (or } \eta_4) = 0.2852315165 \\ \xi_5 \text{ (or } \eta_5) = 0.7650553239 \\ \xi_6 \text{ (or } \eta_6) = 1 \end{array} \right\} \rightarrow (\xi_i, \eta_j), i, j = 1, \dots, 6 \quad (2)$$

Eq. (2) defines the Gauss-Lobatto-Legendre (GLL) points [11]. Thus, a 36-node 2-D spectral plate element can be formulated. It should be pointed out that the nodal coordinates

adopted in the present formulation differ from the ones used by Zak [15], thus the spectral plate element is regarded as a new one, although the same extended form of the displacement field of the plate is used in the formulation.

2. 2 Shape functions

Similar to the conventional finite element method, the generalized displacement field in the 36-node 2-D spectral plate element can be assumed as:

$$q_N^e(\xi, \eta) = \sum_{i=1}^6 \sum_{j=1}^6 N_i(\xi) N_j(\eta) q_N^e(\xi_i, \eta_j) = \sum_{i=1}^6 \sum_{j=1}^6 N_{ij}(\xi, \eta) q_N^e(\xi_i, \eta_j) \quad (3)$$

where $N_{ij}(\xi, \eta) = N_i(\xi) N_j(\eta)$ are shape functions, $q_N^e(\xi_i, \eta_j)$ ($i, j = 1, 2, \dots, 6$) denote the nodal degrees of freedom, and $N_i(\xi)$ and $N_j(\eta)$ are the one-dimensional shape functions in the local $\xi\eta$ coordinate system defined as:

$$N_i(\xi) = \prod_{k=1, k \neq i}^6 \frac{\xi - \xi_k}{\xi_i - \xi_k}; \quad N_j(\eta) = \prod_{k=1, k \neq j}^6 \frac{\eta - \eta_k}{\eta_j - \eta_k}, \quad i, j = 1, \dots, 6 \quad (4)$$

2. 3 Displacement and strain fields

To use a 2-D spectral element to model the 3-D behavior of the Lamb wave propagation in plates, the extended form of the displacement field, proposed by Zak [15], is adopted. The 3-D displacement field of a plate in the global coordinate system (x - y - z) set in the middle plane of the plate can be written as [15]:

$$\begin{aligned} u(x, y, z) &= u_0(x, y) + z \cdot \Phi(x, y) \\ v(x, y, z) &= v_0(x, y) + z \cdot \Psi(x, y) \\ w(x, y, z) &= w_0(x, y) + z \cdot \Omega(x, y) \end{aligned} \quad (5)$$

where u_0 , v_0 and w_0 are the averages of the displacements at the upper and lower surfaces of the plate, Φ , Ψ and Ω are the differences between the displacements at the upper and lower surfaces,

$$\begin{aligned} u_0(x, y) &= \frac{u(x, y, h/2) + u(x, y, -h/2)}{2}, \quad \Phi(x, y) = \frac{u(x, y, h/2) - u(x, y, -h/2)}{h} \\ v_0(x, y) &= \frac{v(x, y, h/2) + v(x, y, -h/2)}{2}, \quad \Psi(x, y) = \frac{v(x, y, h/2) - v(x, y, -h/2)}{h} \\ w_0(x, y) &= \frac{w(x, y, h/2) + w(x, y, -h/2)}{2}, \quad \Omega(x, y) = \frac{w(x, y, h/2) - w(x, y, -h/2)}{h} \end{aligned} \quad (6)$$

where h is the plate thickness. It is seen that there are totally six generalized displacement functions, therefore, each node of the element has six DOFs, namely, $u_0(\xi_i, \eta_j)$, $v_0(\xi_i, \eta_j)$, $w_0(\xi_i, \eta_j)$, $\Phi(\xi_i, \eta_j)$, $\Psi(\xi_i, \eta_j)$, $\Omega(\xi_i, \eta_j)$.

For small strains, the 3-D strain-displacement relations of a plate can be written by:

$$\begin{aligned}
 \varepsilon_x &= \frac{\partial u_0}{\partial x} + z \frac{\partial \Phi}{\partial x}, & \gamma_{yz} &= \frac{\partial w_0}{\partial y} + z \frac{\partial \Omega}{\partial y} + \Psi \\
 \varepsilon_y &= \frac{\partial v_0}{\partial y} + z \frac{\partial \Psi}{\partial y}, & \gamma_{zx} &= \frac{\partial w_0}{\partial x} + z \frac{\partial \Omega}{\partial x} + \Phi \\
 \varepsilon_z &= \Omega, & \gamma_{xy} &= \frac{\partial u_0}{\partial y} + z \frac{\partial \Phi}{\partial y} + \frac{\partial v_0}{\partial x} + z \frac{\partial \Psi}{\partial x}
 \end{aligned} \tag{7}$$

2. 4 Mass and stiffness matrices

For a 36-node 2-D spectral plate element, the displacement field within the plate element can be expressed in the following form:

$$\begin{Bmatrix} u \\ v \\ w \end{Bmatrix} = [N] \{q\} = \sum_{i=1}^6 \sum_{j=1}^6 [N_{ij}(\xi, \eta)] \begin{Bmatrix} u_0(\xi_i, \eta_j) \\ v_0(\xi_i, \eta_j) \\ w_0(\xi_i, \eta_j) \\ \Phi(\xi_i, \eta_j) \\ \Psi(\xi_i, \eta_j) \\ \Omega(\xi_i, \eta_j) \end{Bmatrix} \tag{8}$$

where $[N]$ denotes the matrix of shape functions.

The strain within the element can be expressed as:

$$\begin{Bmatrix} \varepsilon_x \\ \varepsilon_y \\ \varepsilon_z \\ \gamma_{yz} \\ \gamma_{zx} \\ \gamma_{xy} \end{Bmatrix} = [B] \{q\} = \sum_{i=1}^6 \sum_{j=1}^6 [B_{ij}(\xi, \eta, z)] \begin{Bmatrix} u_0(\xi_i, \eta_j) \\ v_0(\xi_i, \eta_j) \\ w_0(\xi_i, \eta_j) \\ \Phi(\xi_i, \eta_j) \\ \Psi(\xi_i, \eta_j) \\ \Omega(\xi_i, \eta_j) \end{Bmatrix} = ([B(\xi, \eta)] + z [\bar{B}(\xi, \eta)]) \{q\} \tag{9}$$

where $[B]$ is the strain matrix, and $\{q\}$ is the nodal displacement vector.

Instead of using the existing GLL quadrature rule [11], the diagonal mass matrix is computed by using Gaussian quadrature as:

$$\begin{aligned}
 m_{II}^e &= \iint_A N_{kp}(\xi, \eta) \mu_L dA = \mu_L \int_{-1}^1 \int_{-1}^1 N_{kp}(\xi, \eta) |J(\xi, \eta)| d\xi d\eta \\
 &\approx \mu_L \sum_{i=1}^3 \sum_{j=1}^3 H_i H_j N_{kp}(\xi_i, \eta_j) |J(\xi_i, \eta_j)| \quad k, p = 1, 2, \dots, 6, \quad I = 6(k-1) + p
 \end{aligned} \tag{10}$$

where $\mu_L = \rho h$ ($L=1,2,3$) and $\mu_L = \rho h^3/12$ ($L=4,5,6$), ρ is the mass density of the material, $|J(\xi, \eta)|$ is the determinant of the Jacobian matrix, H_i, H_j and ξ_i, η_j are weights and abscissas of Gaussian quadrature. Note that the computational effort in obtaining the mass matrix is only about 25 % of that by the existing GLL quadrature rule.

The stiffness matrix can be computed by using Gaussian quadrature as:

$$\begin{aligned}
 [K]^e &= \iint_V \left([B(\xi, \eta)] + z[\bar{B}(\xi, \eta)] \right)^T [D] \left([B(\xi, \eta)] + z[\bar{B}(\xi, \eta)] \right) dV \\
 &= h \int_{-1}^1 \int_{-1}^1 [B]^T [D] [B] |J(\xi, \eta)| d\xi d\eta + \frac{h^3}{12} \int_{-1}^1 \int_{-1}^1 [\bar{B}]^T [D] [\bar{B}] |J(\xi, \eta)| d\xi d\eta \\
 &= h \sum_{i=1}^N \sum_{j=1}^N H_i H_j [B_{ij}(\xi_i, \eta_j)]^T [D] [B_{ij}(\xi_i, \eta_j)] |J(\xi_i, \eta_j)| + \\
 &\quad \frac{h^3}{12} \sum_{i=1}^N \sum_{j=1}^N H_i H_j [\bar{B}_{ij}(\xi_i, \eta_j)]^T [D] [\bar{B}_{ij}(\xi_i, \eta_j)] |J(\xi_i, \eta_j)|
 \end{aligned} \tag{11}$$

where $[D]$ is the elasticity matrix of the material. For an isotropic material, $[D]$ is given by:

$$[D] = \frac{E(1-\nu)}{(1+\nu)(1-2\nu)} \begin{bmatrix} 1 & \frac{\nu}{1-\nu} & \frac{\nu}{1-\nu} & 0 & 0 & 0 \\ & 1 & \frac{\nu}{1-\nu} & 0 & 0 & 0 \\ & & 1 & 0 & 0 & 0 \\ & & & \frac{5(1-2\nu)}{12(1-\nu)} & 0 & 0 \\ & symmetric & & \frac{5(1-2\nu)}{12(1-\nu)} & 0 & \\ & & & & \frac{1-2\nu}{2(1-\nu)} & \end{bmatrix} \tag{12}$$

where E is the modulus of elasticity, ν is Poisson's ratio. A correction factor [16] has been included for calculations of the transverse shear stresses.

2. 4 The time integration scheme

In terms of the spectral plate element, the well-known governing differential equations for the wave propagation in plate structures can be written in the following matrix form,

$$[M]\{\ddot{Q}\} + [K]\{Q\} = \{F\} \tag{13}$$

where $\{Q\}$ is the generalized displacement vector of the structure and the double dots denote the second-order derivative with respect to time t , $[M]$ and $[K]$ are the structural mass matrix and stiffness matrix, and $\{F\}$ is the vector of the time dependent excitation signal, respectively.

Due to the fact that the mass matrix $[M]$ is a diagonal matrix, a crucial reduction of the complexity and the cost of the numerical time integration can be achieved by using central finite difference method [17-18]. Thus, Eq. (13) can be explicitly integrated as follows, namely,

$$\{Q\}_{t+\Delta t} = \Delta t^2 [M]^{-1} \left(\{F\}_t - [K]\{Q\}_t \right) + 2\{Q\}_t - \{Q\}_{t-\Delta t} \tag{14}$$

where t is the time, and Δt denotes the time step of the time integration. When $\Delta t \leq \Delta t_{cr}$, the central finite difference method is stable. $\Delta t_{cr} = 2/\omega_{max}^e$, where ω_{max}^e is the maximum circular

frequency of $\left| [k]^e - \omega^2 [M]^e \right| = 0$. $[k]^e$ and $[M]^e$ are the stiffness and mass matrices of the smallest element in the spectral finite element model.

3. Numerical examples and discussions

Several examples with existing results are investigated to validate the formulations, solution procedures and written programs. Zero initial conditions are assumed for all numerical simulations presented in this paper. It should be pointed out that all existing results used for comparisons are re-produced by the present authors.

3.1 Comparisons with SFE based on Chebyshev polynomials

To compare the new spectral finite element (NSFE) based on the Legendre polynomials with the same kind SFE but based on Chebyshev polynomials (SFE-Chebyshev) [15], consider first the elastic wave propagation in an aluminum thin plate with all four edges free and a geometric configuration of 1000 mm×1000 mm×10 mm shown in Fig. 1. Three special points, denoted by A , E and O , will be used in the discussions. For verifications, material properties and excitation signal are the same as those in [15], namely, Young's modulus $E = 72.7$ GPa, mass density $\rho = 2700$ kg/m³, and Poisson's ratio $\nu = 0.33$, and the excitation signal shown in Fig. 2c is:

$$F(t) = 50 \sin(2\pi t / 10) * \frac{1}{2} (1 - \cos(2\pi t / 60)) \text{ if } 0 \leq t \leq 60 \text{ and } 0 \text{ if } t > 60 \quad (15)$$

where the unit of time t is in micro-seconds (μs). Two loading types shown in Fig. 2a and 2b are considered.

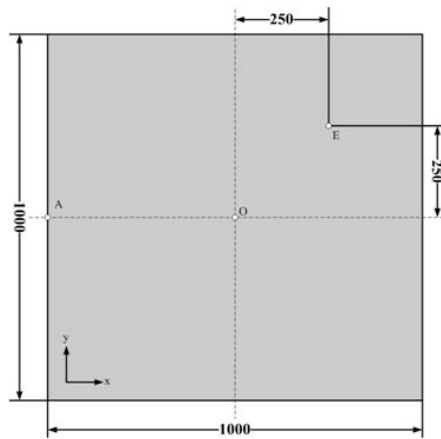


Fig. 1. Geometry of an aluminum plate

A uniform mesh of 50×50 spectral plate elements is used in modeling the aluminum square plate, resulting in 378,006 degrees of freedom, the same as that in [15]. The total time is set to 0.4 ms. For the element with the same size and the same number of nodes, the critical time step is different. $\Delta t_{cr} = 0.188 \mu\text{s}$ for NSFE and $\Delta t_{cr} = 0.103 \mu\text{s}$ for SFE-Chebyshev. Thus, much

larger time increment can be used as compared to SFE-Chebyshev to achieve the same solution accuracy. In turn, the computational efficiency is raised by using the proposed element.

For loading case 1 shown in Fig. 2a, the anti-symmetric Lamb mode A_0 is excited. In the present 2-D plate model, the dual forces are applied at point O along the direction of w_0 . Fig. 3 shows the response of the displacement of the plate at the excitation point O and the boundary point A , and results obtained by both elements are close to each other.

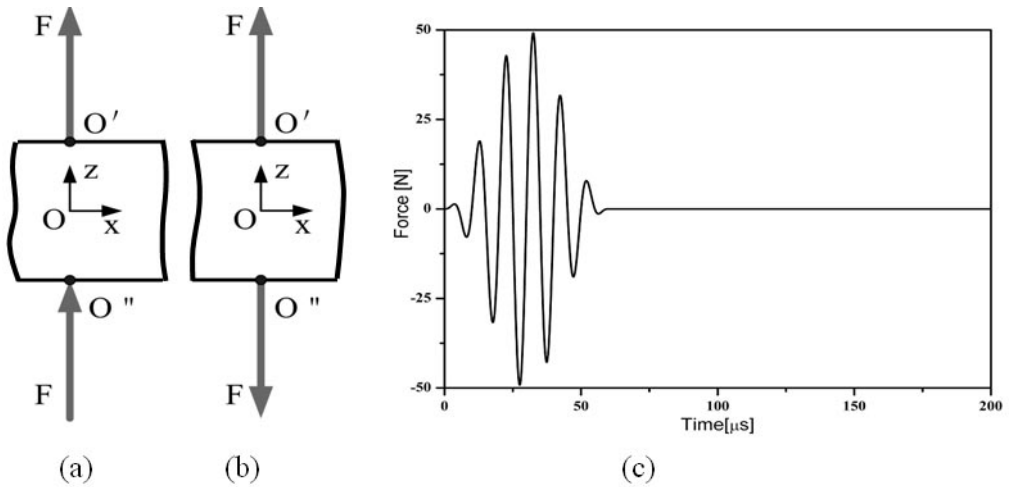


Fig. 2. Loading types and excitation signal in time domain

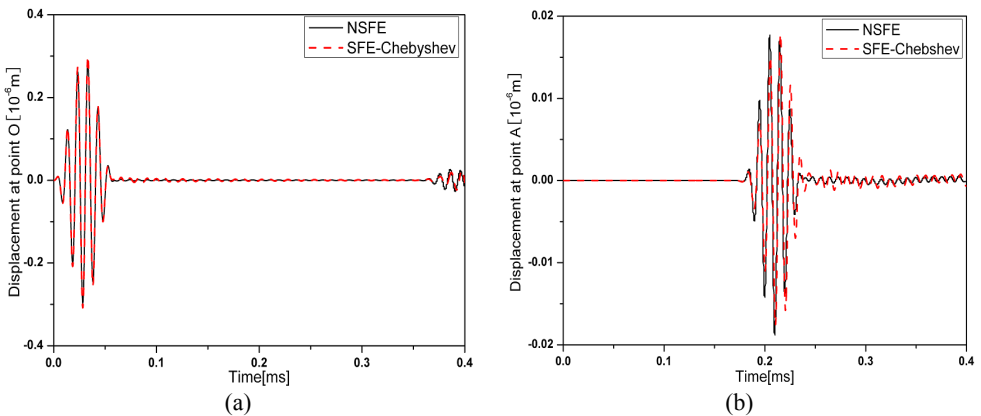


Fig. 3. Response displacement signals at (a) point O and (b) point A for the A_0 mode

For loading case 2 shown in Fig. 2b, dual forces with opposite directions are applied on both the upper and the lower surfaces of the plate at point O , thus the symmetric Lamb mode S_0 is excited. In the 2-D plate model, the dual forces are applied at point O along the direction of the generalized displacement Ω . Fig. 4 shows the response of the displacement of the plate at the excitation point O and the boundary point A . It is observed that results obtained by both elements are again close to each other. Fig. 5 indicates two snap shots at time of 0.08 ms (Fig. 5a) and 0.16 ms (Fig. 5b) and demonstrate the process of wave propagation visually. The reflective waves from the boundaries can be clearly seen in Fig. 5b.

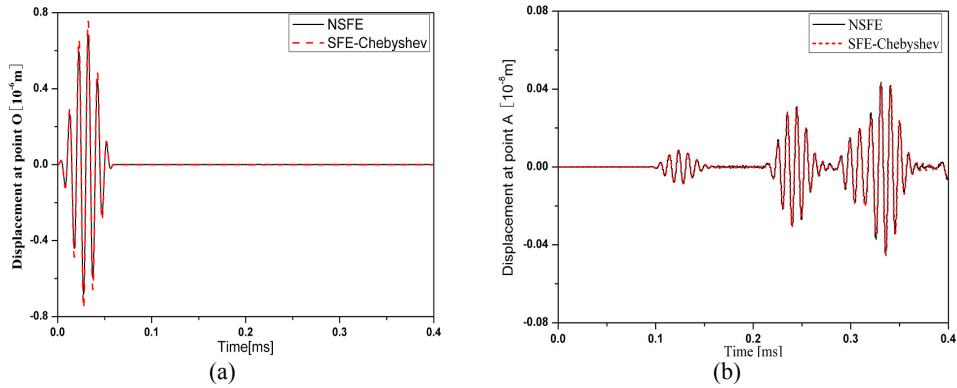


Fig. 4. Response displacement signals at (a) point *O* and (b) point *A* for the S_0 mode

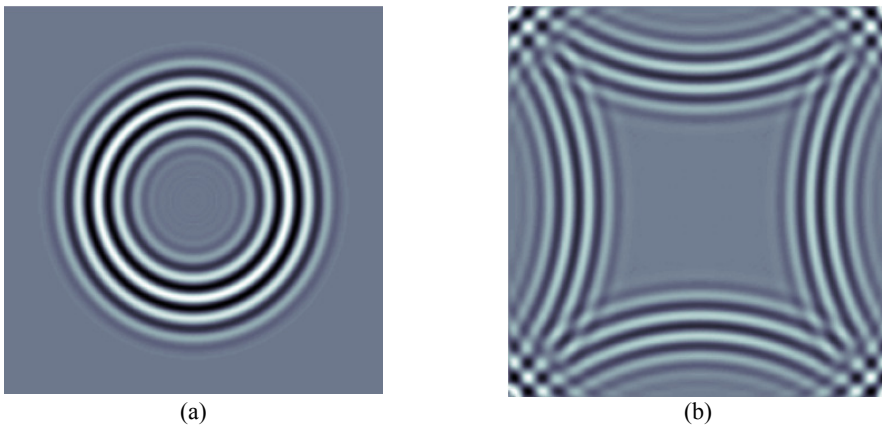


Fig. 5. Propagation of the S_0 mode of Lamb waves in an aluminum plate

3. 2 Comparisons with the 3-D SFE

To compare the new spectral plate element with the 3-D SFE based on the same Legendre polynomials in [13], consider again the elastic wave propagation in an aluminum thin plate shown in Fig. 1. However, the thickness changes to 2 mm and Young’s modulus $E = 71.0$ GPa . Two loading types shown in Fig. 6a and 6b are considered. The excitation signal shown in Fig. 6c is given by:

$$F(t) = \sin(2\pi t / 5) * (1 - \cos(2\pi t / 25)) / 2 \quad \text{for } 0 \leq t \leq 25 \text{ and } 0 \text{ for } 25 < t \quad (16)$$

where the unit of time t is in micro-seconds (μs).

For comparisons, the aluminum plate under investigation is meshed by 100×100 . For the new spectral finite elements, there are total of 1,506,006 degrees of freedom. For the 3-D SFE [13], three points are used in the thickness direction ($6 \times 6 \times 3$) thus there are a total of 2,259,009 DOFs. For the same size element, the critical time step is different. $\Delta t_{cr} = 0.117 \mu\text{s}$ for NSFE (6×6) and $\Delta t_{cr} = 0.098 \mu\text{s}$ for 3-D SFE. The total calculation time is set to 0.3 ms. Thus, NSFE needs 3000 time steps and 3-D SFE uses 4000 time steps [13] to achieve similar accuracy, since the thickness of the plate is only 2 mm.

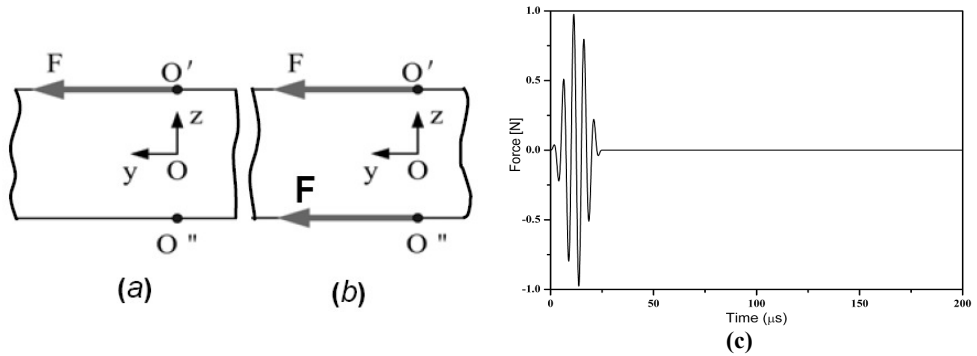


Fig. 6. The loading types and excitation signal in time domain

For loading case 3 shown in Fig. 6a, both symmetric mode S_0 and anti-symmetric mode A_0 are excited. In the 2-D plate model, the force is applied at point O along the direction of the displacement components v_0 and Ψ . Fig. 7a shows the response of the displacement v of the plate recorded at point E . It is observed that results obtained by the two methods are comparable but have slight differences at certain time instants. Perhaps this might be caused by the slightly different distributions of the in-plane displacements along the thickness direction.

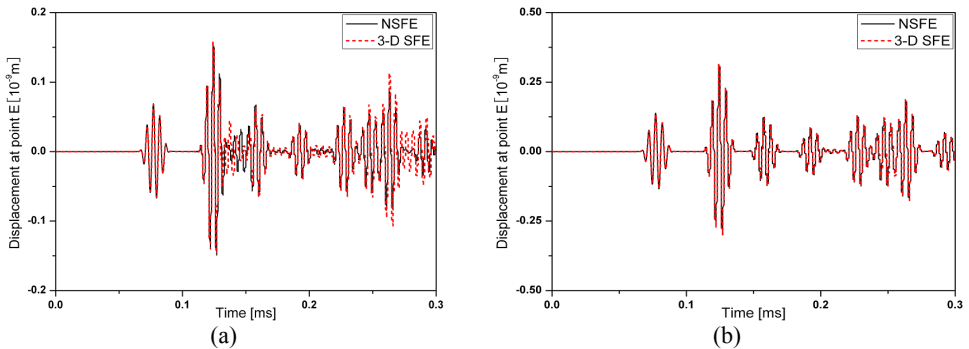


Fig. 7. Response signals of displacement v at point E

For loading case 4 shown in Fig. 6b, only the symmetric Lamb mode S_0 is excited. In the 2-D plate model, the dual forces are applied at point O along the y direction. Fig. 7b shows the response of the displacement v of the plate recorded at point E . It is observed that results obtained by the two methods are close to each other.

3.3 Damage detection by using the NSFE method

In this section, a plate with damages shown in Fig. 8 is considered. The dimension and material parameters are the same as those given in Section 3.1. There are two damage zones: $d1$ and $d2$. The damage zone $d1$ has the dimensions of length 40 mm and width 20 mm and the damage zone $d2$ has the dimensions of length 20 mm and width 20 mm. Load case 1 is used in the simulation. The plate is modeled by 100×100 36-node NSFEs. The damage is modeled by simply reducing the element stiffness [19]. In the simulation, modulus of elasticity in the damaged area is reduced to 10 % of the modulus of elasticity in the undamaged area. The total calculation time is set to 0.8 ms so the reflected waves from the damage can reach all measuring points (points B , C , D and E). The time increment is set to 10^{-7} s.

Consider first only the damage $d1$ existing in the plate. Fig. 9 shows a snapshot at time instant 0.016 ms. The reflected wave from the damage can be clearly observed. For damage detection, the displacement responses at points B , C , D and E depicted in Fig. 8 are recorded. The responses of undamaged plate are then subtracted from the corresponding responses of the damaged plate. The differences of responses are plotted in Fig. 10. Based on the time interval, the wave propagation speed, as well as the location of points B , C , D and E , the location of the damage can be determined by using the method presented in [12].

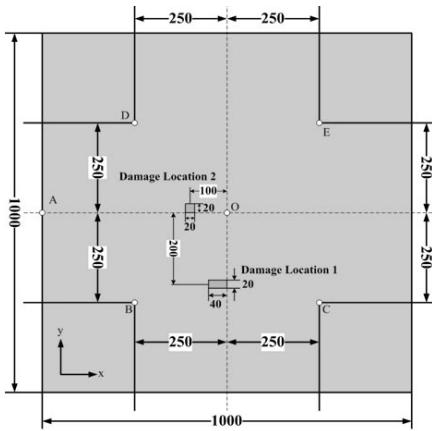


Fig. 8. A square plate with damages

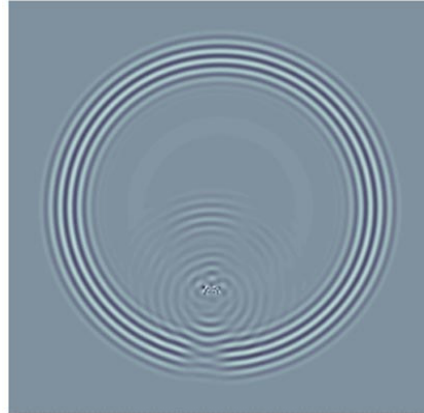
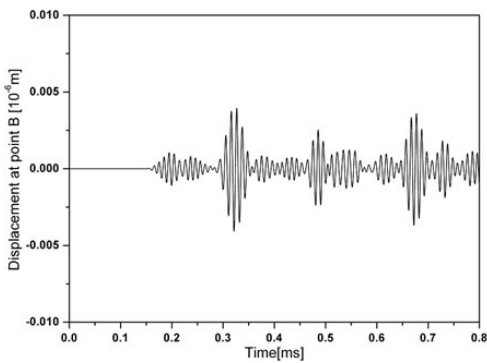
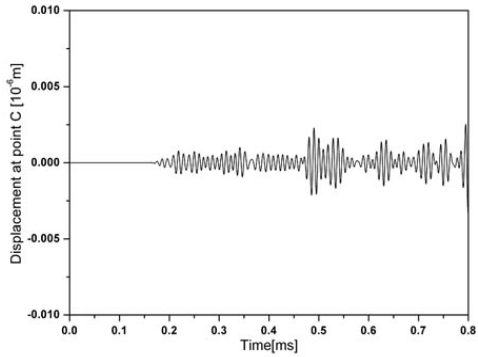


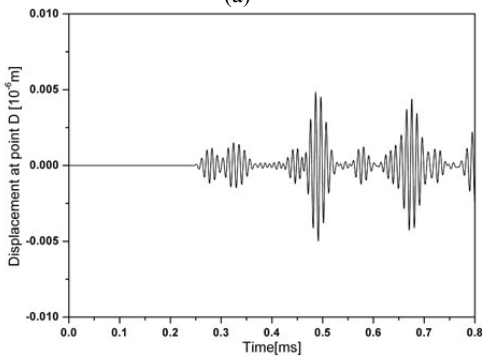
Fig. 9. Snapshot at time of 0.016 ms



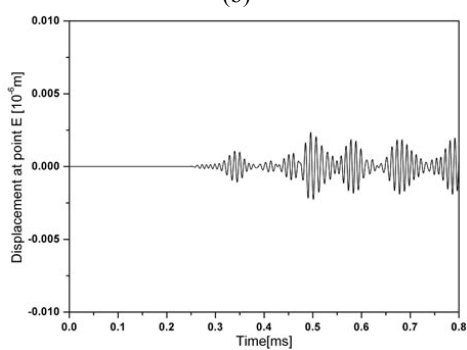
(a)



(b)



(c)



(d)

Fig. 10. Difference response signals of plate with damage $d1$ at point (a) B , (b) C , (c) D , (d) E

Consider next two damages exist in the plate. Fig. 11 shows three snapshots at different time instances to demonstrate the processes of the wave propagation. The reflected waves from both damages are clearly observed. Similarly, the displacement responses at points *B*, *C*, *D* and *E* are recorded for damage detection; the responses of undamaged plate are then subtracted from the corresponding responses of the damaged plate which are shown in Fig. 12. Based on the time interval, the wave propagation speed, as well as the location of points *B*, *C*, *D* and *E*, the location of the damages can be determined by using the method presented in [12].

Comparison of results provided in Fig. 10 and Fig. 12 indicates obvious difference due to different damages existing in the plates.

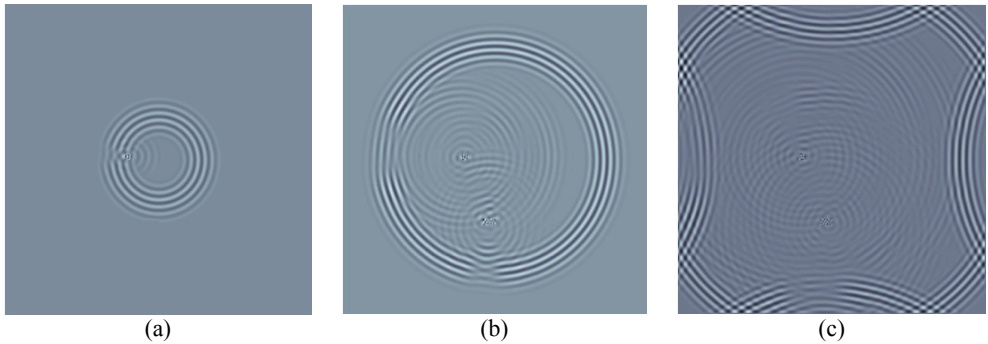


Fig. 11. Propagation of the A_0 mode Lamb waves in an aluminum plate with damages

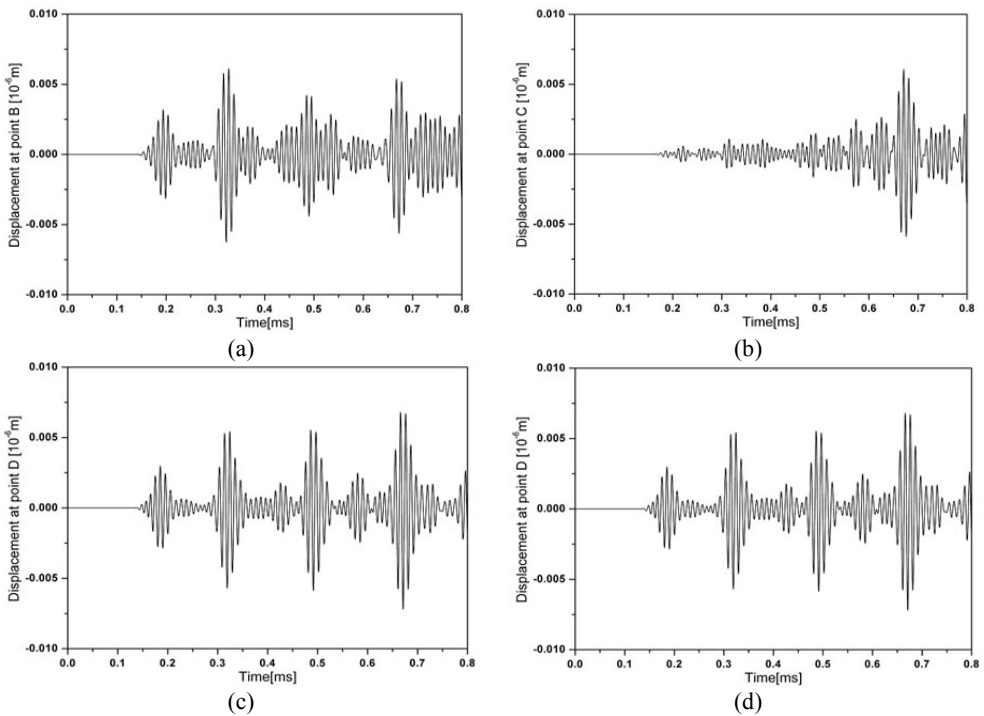


Fig. 12. Difference response signals of plate with damages at point (a) *B*, (b) *C*, (c) *D*, (d) *E*

4. Conclusions

In this paper, a new spectral plate element is proposed for modeling selectively or simultaneously the symmetric and/or anti-symmetric modes of Lamb waves propagating in plates. The extended form of the displacement field and the Legendre polynomials are adopted in the formulation. A simple way to formulate the diagonal mass matrix is used to reduce further the computational effort. Formulations are given in detail. Various numerical simulations have been carried out for aluminum plates with and without damage by using the proposed spectral plate element. Comparisons of simulated results to existing results verified the formulations. The feature of the proposed element, i.e., modeling selectively symmetric and/or anti-symmetric modes of Lamb waves propagating in plates, has been demonstrated. It is demonstrated that the proposed spectral plate element is more effective than the spectral plate element based on Chebyshev polynomials and the 3-D spectral finite element based on the same order of Legendre polynomials. Since the damage location can be also identified from the simulated transmitted and reflected waves by using the method presented in [12], therefore, the new spectral plate element may be useful in the area of Lamb-wave based structural health monitoring.

Acknowledgements

The work is partially supported by the National Natural Science Foundation of China (50830201) and by the Priority Academic Program Development of Jiangsu Higher Education Institutions.

References

- [1] **Kim Y., Ha S., Chang F. K.** Time-domain spectral element method for built-in piezoelectric-actuator-induced Lamb wave propagation analysis. *AIAA Journal*, Vol. 46, Issue 3, 2008, p. 591–600.
- [2] **Cho Y., Rose J. L.** A boundary element solution for a mode conversion study on the edge reflection of Lamb waves. *Journal of Acoustical Society of America*, Vol. 99, Issue 4, 1996, p. 2097–2109.
- [3] **Delsanto P. P., Mignogna R. B.** A spring model for the simulation of the ultrasonic pulses through imperfect contact interfaces. *Journal of Acoustical Society of America*, Vol. 104, 1998, p. 1–8.
- [4] **Delsanto P. P., Whitecomb T., Chaskelis H. H., et al.** Connection machine simulation of ultrasonic wave propagation in materials. I: The one-dimensional case. *Wave Motion*, Vol. 16, 1992, p. 65–80.
- [5] **Wang X., Xu C. L., Xu S. M.** The discrete singular convolution for analyses of elastic wave propagations in one-dimensional structures. *Applied Mathematical Modelling*, Vol. 34, 2010, p. 3493–3508.
- [6] **Komatitsch D., Barnes C. H., Tromp J.** Simulation of anisotropic wave propagation based upon a spectral element method. *Geophysics*, Vol. 4, 2000, p. 1251–1260.
- [7] **Igawa H., Komatsu K., Yamaguchi I., et al.** Wave propagation analysis of frame structures using the spectral element method. *Journal of Sound and Vibration*, Vol. 277, 2004, p. 1071–1081.
- [8] **Palacz M., Krawczuk M., Ostachowicz W.** The spectral finite element model for analysis of flexural-shear coupled wave propagation. Part 1: Laminated multilayer composite. *Composite Structures*, Vol. 68, 2005, p. 37–44.
- [9] **Sun H., Zhou L.** Analysis of damage characteristics for cracked composite structures using spectral element method. *Journal of Vibroengineering*, Vol. 14, Issue 1, 2012, p. 430–439.
- [10] **Seriani G.** 3-D large scale wave propagation modeling by spectral element method on Cray T3E multiprocessor. *Computer Methods in Applied Mechanics and Engineering*, Vol. 164, Issue 1-2, 1998, p. 235–247.
- [11] **Kudela P., Krawczuk M., Ostachowicz W.** Wave propagation modeling in 1D structures using spectral finite elements. *Journal of Sound and Vibration*, Vol. 300, 2007, p. 88–100.

- [12] **Zak A., Krawczuk M., Ostachowicz W.** Propagation of in-plane waves in an isotropic panel with a crack. *Finite Elements in Analysis and Design*, Vol. 42, 2006, p. 929–941.
- [13] **Peng H. K., Meng G., Li F. C.** Modeling of wave propagation in plate structures using three-dimensional spectral element method for damage detection. *Journal of Sound and Vibration*, Vol. 320, 2009, p. 942–954.
- [14] **Kudela P., Zak A., Krawczuk M., et al.** Modeling of wave propagation in composite plates using the time domain spectral element method. *Journal of Sound and Vibration*, Vol. 302, 2007, p. 728–745.
- [15] **Zak A.** A novel formulation of a spectral plate element for wave propagation in isotropic structures. *Finite Elements in Analysis and Design*, Vol. 45, 2009, p. 650–658.
- [16] **Vinson J. R., Sierakowski R. L.** *Behavior of Structures of Composite Materials*. Martinus Nijhoff, 1989.
- [17] **Komatitsch D., Martin R., Tromp J., et al.** Wave propagation in 2-D elastic media using a spectral element method with triangles and quadrangles. *Journal of Computational Acoustics*, Vol. 9, Issue 2, 2001, p. 703–718.
- [18] **Subbaraj K., Dokainish M. A.** A survey of direct time-integration method in computational structural dynamic. I. Explicit methods. *Computers & Structures*, Vol. 32, Issue 6, 1989, p. 1371–1386.
- [19] **Fraswell M. I., Penny J.** Crack modeling for structural health monitoring. *Structural Health Monitoring*, Vol. 1, Issue 2, 2002, p. 139–148.